SERS-active linear barcodes by microfluidic-assisted patterning

Sami Pekdemir[a,b], *Hasan Hüseyin Ipekci*[b,c], *Murat Serhatlioglu*[d], *Caglar Elbuken*[d,e*], *M. Serdar Onses*[a,b,d*]

[a] Department of Materials Science and Engineering, Erciyes University, Kayseri, 38039, Turkey

[b] ERNAM - Erciyes University Nanotechnology Application and Research Center, Kayseri, 38039.

[c] Metallurgical and Materials Engineering, Faculty of Engineering and Architecture, Necmettin Erbakan University, Konya, Turkey

[d] UNAM−National Nanotechnology Research Center, Institute of Materials Science and Nanotechnology, Bilkent University, 06800, Ankara, Turkey

[e] Faculty of Biochemistry and Molecular Medicine, Faculty of Medicine, University of Oulu, 90014 Oulu, Finland.

* Address correspondence to: onses@erciyes.edu.tr, elbuken@unam.bilkent.edu.tr

ABSTRACT

Simple, low-cost, robust and scalable fabrication of microscopic linear barcodes with high levels of complexity and multiple authentication layers is critical for emerging applications in information security and anti-counterfeiting. This manuscript presents a novel approach for fabrication of microscopic linear barcodes that can be visualized under Raman microscopy. Microfluidic channels are used as molds to generate linear patterns of end-grafted polymers on a substrate. These patterns serve as templates for area-selective binding of colloidal gold nanoparticles resulting in plasmonic arrays. The deposition of multiple taggant molecules on the plasmonic arrays via a second microfluidic mold results in a linear barcode with unique Raman fingerprints that are enhanced by the underlying plasmonic nanoparticles. The width of the bars is as small as 10 μm, with a total barcode dimension on the order of 100 μm. The simultaneous use of geometric and chemical security layers provides a high level of complexity challenging the counterfeiting of the barcodes. The additive, scalable, and inexpensive nature of the presented approach can be easily adapted to different colloidal nanomaterials and applications.

KEYWORDS: anti-counterfeiting, SERS, plasmonics, microfluidics, colloidal nanoparticles

1. Introduction

Barcodes are one of the most widely used approaches to encode information on a surface. The basis of barcodes is coding of numbers and letters into compact-sized labels, which consist of symbols spatially defined on a surface. Linear barcodes that are composed of a series of bars of varying widths separated by spaces are commonly utilized to track objects that range from simple merchandises to important documents [1]. These barcodes can be simply printed on paper and verified by scanners. This simplicity challenges their employment for the protection of valuable products or information-rich documents since it is straightforward to duplicate such visual barcodes. A first-order approach to increase the level of complexity is incorporating additional layers of security. The size-dependent properties of nanomaterials offer unique opportunities in fabricating barcodes with a precisely defined response based on various optical phenomena, including fluorescence, scattering, and absorbance [2,3]. In particular, fluorescence-based security labels have attracted significant interest. For example, the size-dependent luminescence from quantum dots is an effective means to increase the complexity of barcodes [4,5]. Both down-conversion [6] and up-conversion [7] emitters, as well as their combinations [8], have been employed for the fabrication of security labels. Besides the emission wavelength, fluorescence lifetime [9] has been utilized as an encoding modality. The broad usage of fluorescence-based encoding of surfaces makes these technologies vulnerable to ever more sophisticated counterfeiters. This issue strongly motivates development of barcodes with a size and authentication mechanism that is difficult to counterfeit.

Plasmonic metallic nanostructures present advanced routes for the fabrication of encoded surfaces. The basis of this capability arises from the unique size, shape, and composition-dependent interaction of nanostructures with light. For example, assembling different sizes of nanocubes onto templates prepared by electron beam lithography resulted in surfaces that have been encoded with spatially defined light absorption [10]. In another recent work [11], the light scattered by randomly positioned metallic nanoparticles (NPs) was utilized in the fabrication of encoded surfaces. Another unique characteristic of metallic nanostructures is the enhancement of fluorescence and Raman scattering [12,13]. Raman scattering

relies on inelastic scattering of light that is based on inherent vibrations of molecules. This material-dependent behavior offers unique opportunities in the fabrication of Raman-active barcodes. The low probability of Raman scattering is a challenge, which results in extremely low intensity levels [14]. Surface-enhanced Raman scattering (SERS) provides electromagnetic and chemical enhancement, addressing this fundamental challenge [15,16].

SERS-based encoded surfaces have been demonstrated to be highly effective for fabricating security labels [17]. In a series of valuable contributions, [18,19] Ling and coworkers have demonstrated the potential of SERS-active barcodes using spatially defined plasmonic structures fabricated by two-photon lithography followed by evaporation of metallic structures. Besides the geometric and vibrational coding, polarization [20] and z-dependence [21] of Raman scattering of multiple taggant molecules have been employed as novel routes for security labels. In a recent work, Li et al. [22] demonstrated facile fabrication of linear SERS barcodes with a length of ~5 cm based on the assembly of colloidal silver nanocubes assisted with a stencil mask. These studies highlight the significant potential of SERS-based barcodes. It is highly desirable to fabricate SERS barcodes at microscopic length scales using colloidal NPs via scalable, low-cost, and robust fabrication approaches.

In the following, we present a purely additive and scalable approach to fabricate SERS-active linear barcodes. Microfluidic channels are employed as molds for patterned deposition of poly(ethylene glycol) (PEG) and Raman-active taggant molecules. First a microfluidic mold is used for patterned deposition of end-grafted PEG. A brief thermal annealing step allows grafting of these polymers onto the substrate surface resulting in linear templates for subsequent attachment of colloidal gold NPs. A second microfluidic mold is placed on the substrate to deposit Raman-active taggant molecules to define linear barcodes. The additive nature of the microfluidic molds allows the deposition of multiple taggant molecules at the desired locations with a high resolution. The result is microscopic linear barcodes that are geometrically and chemically protected against counterfeiting. An advantage of the presented approach is the robustness of the plasmonic barcodes, thanks to the strong binding of colloidal NPs to the end-grafted polymer layers.

2. Experimental

2.1. Materials

Silicon wafers (<100>, N/Phos) were purchased from Wafer World Inc. Sylgard 184 silicone elastomer kit from Dow Corning was used for the fabrication of polydimethylsiloxane (PDMS) molds. PEG (35.0 kg/mol, PDI: 1.02, BioUltra), methylene blue (MB) (purity 97%), chloroform (purity 99%) and rhodamine 6G (R6G) (purity >95%) were purchased from Sigma-Aldrich. SU-8 2005 photoresist was purchased from MicroChem. Ethanol (purity 99%), methylene orange (MO) (ACS, reagent grade), N,N-Dimethylformamide (DMF) (purity 99.8%) were purchased from Merck. Citrate stabilized gold NPs were obtained from Ted Pella Inc.

2.2. Characterization

The topography of the surface was analyzed with AFM (Veeco Multimode 8) in tapping mode. The morphology of the substrate after immobilization of the gold NPs was analyzed using SEM imaging (Zeiss EVO LS10) that is performed at 20 kV. SERS measurements were taken on a WITec alpha M+ confocal Raman microscopy system equipped with 50× objective and 532 nm laser source (2 μm spot size, 0.1 mW power).

2.3. Fabrication of PDMS Molds

We designed multiple molds for patterned deposition of PEG and Raman-active taggant molecules. These molds resulted in linear barcodes in Code 93 system, when used sequentially for PEG and taggant molecules,

Optical lithography masks for silicon master fabrication were designed using L-Edit CAD software. The designs were transferred to a mask writer (Heidelberg DWL 2000) and laser-printed on a 5 inch Cr/fused silica transparency photomask. Then, SU-8 2005 photoresist was spin-coated

(acceleration: 500 rpm/s, speed: 2500 rpm/s, time: 40 s) on a 4 inch diameter silicon wafer to obtain 5 µm resist thickness and prebaked on a hot plate at 65 °C for 1 min and 95 °C for 3 min. Then, SU-8 layer was exposed to UV light under a mask aligner (EVG 620) at 80 mJ/cm^2 intensity and post-baked on a hot plate at 65 °C for 2 min and 95 °C for 3 min. Finally, the resist was developed for 45 s and dried by nitrogen purge. For PDMS casting, we used a 15:1 base polymer to curing agent ratio to improve adhesion to the substrate during molding process. The PDMS mixture was prepared, degassed, and poured onto the SU-8 master and cured on a hot plate for 5 h at 80 °C. Finally, the cured PDMS was peeled off from the SU-8 master, and inlet/outlet holes (1 mm diameter) were punched using a biopsy puncher. We aligned the PDMS mold to a bare silicon surface and brought them in contact without any plasma treatment. To prevent any leakage, we sandwiched the silicon/PDMS structure between two flat 3 mm-thick PMMA slabs, which were prepared using a CO_2 laser cutter (Epilog Zing 30 W CO_2 laser), in vector cutting mode at 1000 dpi, 10 W power, 5 kHz frequency, and 5 mm/s translation speed.

2.4. Patterning of PEG and taggant molecules via PDMS molds

The PDMS molds were washed in DMF under sonication for 10 min and then dried at 90 °C for 2 h. The molds were then placed onto silicon substrates that were freshly cleaned in a UV-ozone chamber (Bioforce, procleaner) for 20 min. A solution (~5 µL) of 6% w/w PEG in water was pipetted to the inlet of microfluidic channels and withdrawn from the outlet with the aid of a syringe pump. After the solvent evaporated, the PDMS mold was gently separated from the substrate, leaving behind linear arrays of PEG. To graft these PEG layers onto the surface, the patterned substrates were annealed in a glove box filled with argon at 180 °C for 5 min. After annealing, the substrates were washed in chloroform, resulting in patterned end-grafted PEG layers, which were dried with nitrogen before use.

For assembly of plasmonic NPs on the patterned surface, a 150 μL volume droplet of citrate-stabilized gold NPs was spotted on the patterned substrate and kept in a humid environment for 1 h. The substrate was then washed in water under sonication for 2 min to remove excess and non-specifically bound particles and dried with nitrogen.

For the patterned deposition of Raman active taggant molecules, we first prepared solutions of R6G (100 μM), MB (1 mM), and MO (1 mM) in a co-solvent system consisting of 95% water and 5% ethanol. The solutions of taggant molecules were withdrawn to the channels with the aid of a syringe pump from the outlet. The mold was removed from the substrate slowly, to minimize damage to the patterned substrate.

2.5. SERS measurements and characterization of security labels

SERS measurements were performed after drying of the solvent. Unless otherwise stated, the taggant molecule is R6G, with a concentration of 100 μM throughout the study. To illustrate the homogeneity of the immobilized plasmonic gold NP arrays, SERS measurements were performed with mapping mode on an area of 25 µm × 60 µm with a step size of 0.5 µm and an integration time of 0.05 s. Each raw spectrum was baseline corrected before further analysis.

3. Results and discussion

Our approach to fabrication of SERS-active linear barcodes relies on microfluidic-assisted patterning of end-functional polymers and taggant molecules (Figure 1). In this approach, a soft PDMS mold is fabricated using masters with features defined via photolithography. The placement of this mold on a substrate results in formation of a network of microchannels that are connected to inlets and outlets. As originally developed by Whitesides and coworkers, ink materials that are dissolved in a solvent can passively fill these channels by capillary action, a process commonly

referred as micromolding in capillaries (MIMIC) [23]. The evaporation of solvent followed by removal of the mold results in patterned arrays of materials. In MIMIC, arrays of linear channels are filled by spotting ink solutions near the open ends of the channels. Advanced forms of this approach involve multiple inlets enabling patterning of different materials [24]. As opposed to passive capillary filling, active filling allows rapid filling of the microchannels with minimal dependence on the channel surface properties and viscosity of the solution. Active filling is especially critical for robust fabrication when working with high vapor pressure solutions. In this study, we employ an active filling strategy with three different molds on the same substrate for patterning end-functional polymer and Raman-active taggant molecules (Figure 1). We first fabricate linear arrays of plasmonic NPs by microfluidic-assisted patterning of end-functional PEG (Figure 1a) using Mold 1. After end-grafting the polymer via thermal annealing, these patterns serve as binding sites for the assembly of colloidal gold NPs. These linear arrays are SERS-active sites for two different barcode designs. To generate Raman-active regions in the geometry of barcodes of Code 93 system, we designed and fabricated two additional PDMS molds referred as Mold 2 and 3 (Figure 1b and 1c). These molds were placed orthogonal to the long-axis of the plasmonic arrays and were used to pattern Raman-active taggant molecules. In this design, the width of the plasmonic linear features determines the height of the linear barcode (Figure 1b and 1c), whereas the individual bars are defined by taggant molecules.

The approach here is that at properly chosen concentrations of Raman-active taggant molecules, intense and selective Raman signals will only arise in the intersections of the taggant molecules with the plasmonic arrays. This approach is key in fabricating discontinuous patterns in the geometry of linear barcodes via a microfluidic-assisted patterning approach. We patterned an exemplary barcode of characters A, B, and C in Code 93 system. In Barcode I (Mold 2, Figure 1b),

each character consists of a different Raman-active taggant molecule with a unique set of molecular vibrations. In the second design referred as Barcode II (Mold 3, Figure 1c), each character is composed of two types of taggant molecules.

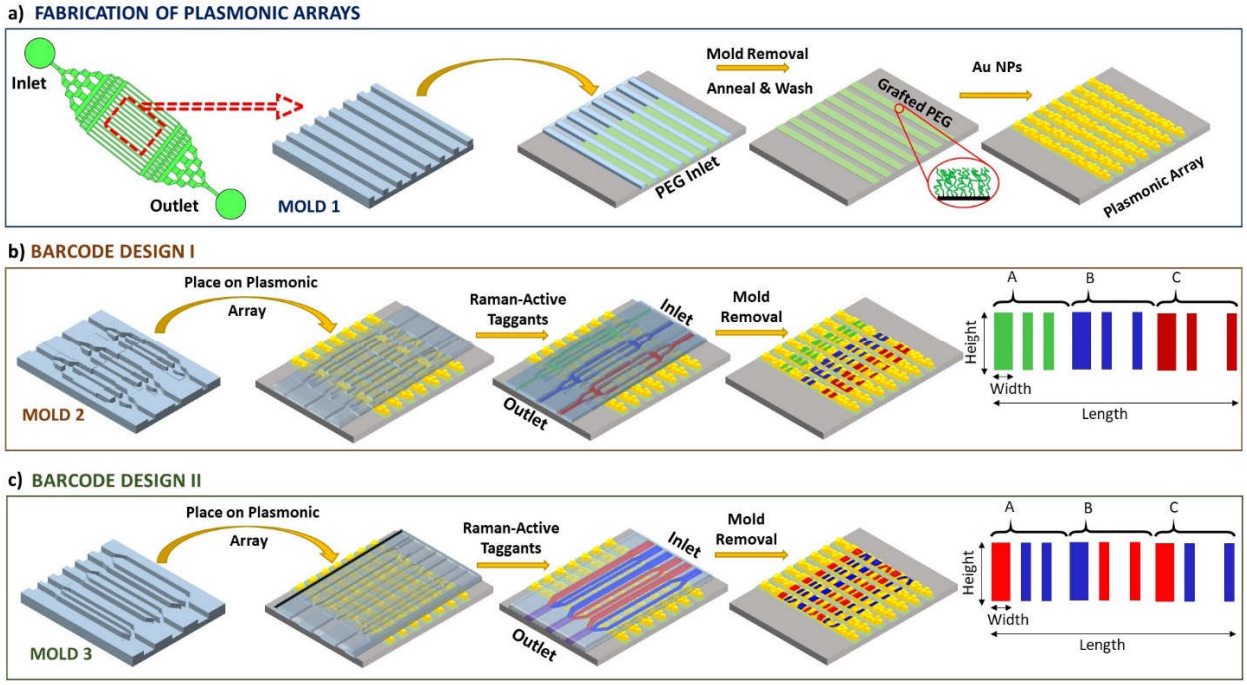

Figure 1. SERS-active linear barcodes by microfluidic molding. a) Linear arrays of plasmonic NPs are first fabricated by deposition of end-functional PEG through microfluidic Mold 1. The removal of Mold 1 is followed by thermal annealing to graft PEG chains onto the silicon substrate. Washing away excess material reveals linear arrays of end-grafted PEG. Plasmonic arrays are obtained by selective assembly of colloidal gold NPs through drop-casting followed by sonication in water. b,c) Two types of barcodes are fabricated on the plasmonic arrays using b) Mold 2, and c) Mold 3. In both cases, the molds are used for area selective deposition of Raman-active taggant molecules that consist of R6G, MB, and MO.

Fabrication and characterization of the plasmonic array

Figure 2 presents schematic description and key results on the fabrication of the plasmonic patterns on a silicon or glass substrate. Our approach relies on linear arrays of end-grafted PEG layers for site-specific adsorption of colloidal gold NPs. Mold 1 was placed on a freshly cleaned substrate leading to microfluidic channels. An aqueous solution of PEG was supplied from the inlet, whereas the outlet was subjected to vacuum using a syringe pump in withdrawal mode to ensure complete filling of the channels (Figure 2a). The microfluidic mold was designed with multiple parallel channels and enables generation of multiple barcodes at a single run (See supporting information). The length, width, and height of the microchannels are 1000, 20, and 5 µm, respectively. After the complete filling of the channels, the tubing was removed from the PDMS mold for solvent evaporation. Then, the PDMS mold was gently removed and the patterned PEG was obtained (Figure 2b). The compliant nature of PDMS enables large area patterning of end-functional polymers (Figure 2e). AFM imaging (Figure 2f) confirms the deposition of PEG over the regions defined by the microfluidic channels. The patterned substrate was annealed under an inert environment at 180 ^{o}C for 5 min to graft the polymer chains onto the surface. Unbound polymers were washed under sonication. Drying of the substrate results in patterned end-grafted layers with in-plane dimensions defined by the microfluidic channel and the out-of-plane dimension set by the length of chains and grafting density (Figure 2c). The height of the end-grafted PEG layers was 8 nm (Figure 2g), with a grafting density of 0.15 chains/nm^2 (see supporting information). This suggests a moderate-density brush regime [25]. The selective adsorption of gold NPs was facilitated by dropping an aqueous solution on the patterned region (Figure 2d). After the immobilization process, the substrate was washed under sonication resulting in strongly bonded robust plasmonic arrays on the end-grafted PEG layer (Figure 2h).

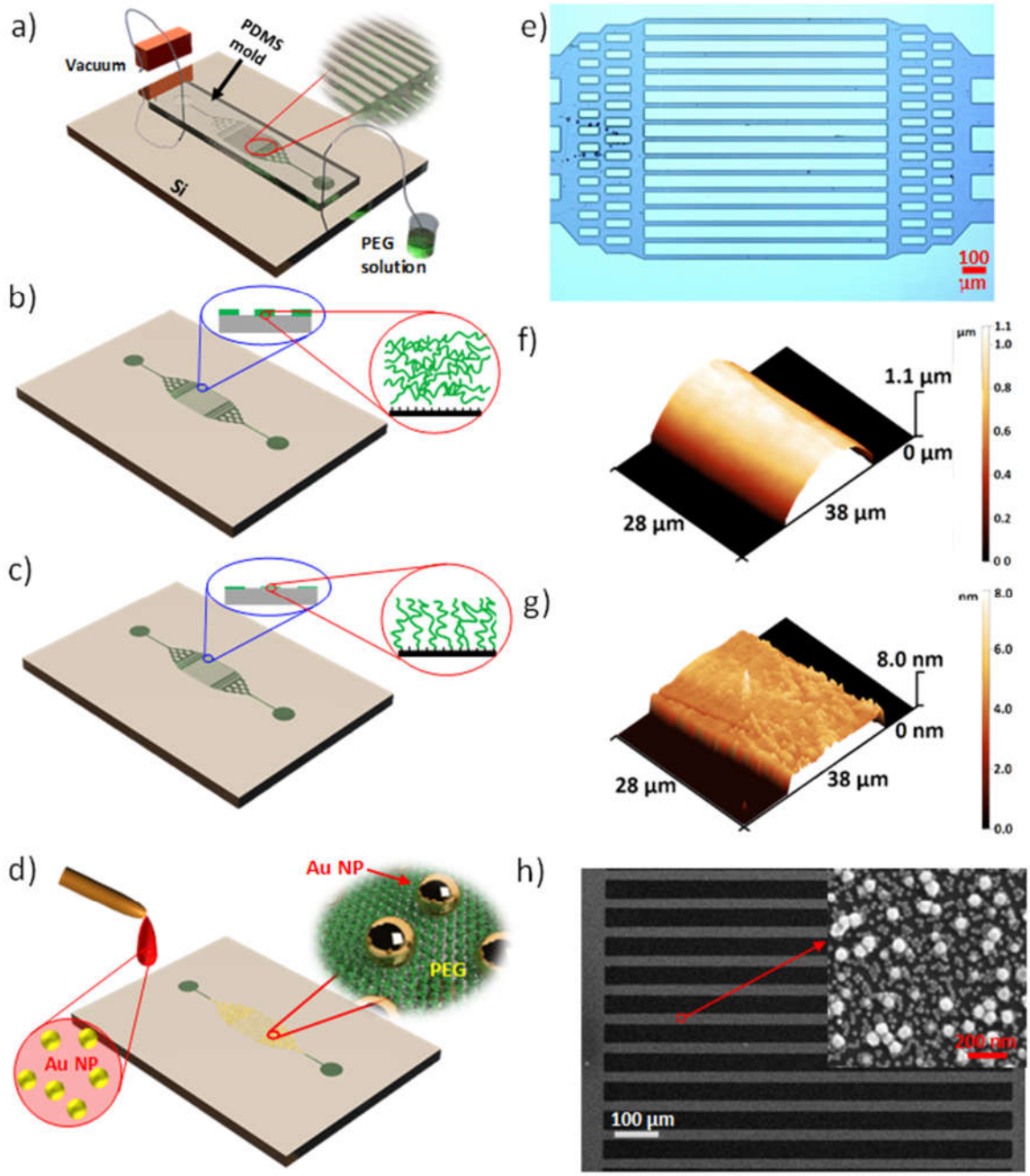

Figure 2. Fabrication of plasmonic arrays using Mold 1. a-d) Schematic illustration of the process. a) Hydroxyl-terminated PEG is deposited through the mold. b) Following evaporation of the solvent and removal of the mold, patterns of PEG are obtained. c) A brief thermal annealing followed by washing leads to end-grafted PEG layers in regions defined by the microfluidic channels. d) A droplet of colloidal gold NP solution is placed on the patterned region followed by

washing under sonication in water. This process is repeated with spherical gold NPs with a diameter of 60 nm and 20 nm, respectively. The immobilization of gold NPs is depicted in the schematic. e-h) Characterization of the patterns. e) Optical microscope image of the patterned PEG polymers via Mold 1. f) AFM image of an individual deposited linear feature. g) AFM image of the end-grafted PEG layers with a thickness of 8 nm. h) SEM image of the plasmonic arrays of gold NPs on the end-grafted PEG layers.

Selective adsorption of colloidal gold NPs on the patterns of end-grafted PEG layers prepared by thermal annealing and washing of the substrates results in plasmonic arrays over large areas (Figure 2h). SEM images showed uniform immobilization of the arrays of gold NPs. The plasmonic arrays were constructed from gold NPs of two different sizes: 60 and 20 nm in diameter. This type of arrangement of gold NPs enables high SERS activity, thanks to the focusing of electromagnetic fields in regions between two particles of varying sizes [24, 25]. To increase the density of the particles that are adsorbed on the end-grafted PEG layer, the gold NPs were immobilized on the surface at five repetitive cycles. Each cycle consisted of drop-casting of gold NPs, incubation and washing under sonication. 60 nm diameter particles were immobilized first, as the density of adsorbed gold NPs increases with the decreasing size of the colloidal particle. The immobilization densities of gold NPs on PEG patterns were calculated from SEM images as 33 ± 2 NP/μm^2 for 60 nm and 635 ± 45 NP/μm^2 for 20 nm particles.

SERS Barcodes: Patterning of taggant molecules on plasmonic arrays.

Linear barcodes employ a series of lines and spaces to encode information on a surface. These barcodes are also referred as one dimensional, since the lines and spaces are positioned along a

single axis [28]. Among several conventions, Code 93 [29] uses three bars with varying widths and spacings to represent alphanumeric characters (Table S1). It has been previously demonstrated that Code 93 can be effectively used for SERS based linear barcodes [22]. A challenge associated with microfluidic molding-based approaches in fabrication of linear barcodes is the inability to pattern discontinuous features [30,31]. To circumvent this issue, we employ a sequential patterning process first to generate binding sites for plasmonic NPs (Mold 1) and then to pattern Raman-active molecules (Mold 2 or 3). Mold 2 and 3 are used to deposit taggant molecules with linear features designed with line widths and separation distances that match the barcode design. Barcodes were chosen to represent ABC letters in Code 93 convention. Molds 2 and 3, consisting of barcode features, are placed in a direction that is orthogonal to the long axis of the plasmonic array (See supporting information).

Mold 2 enables simultaneous patterning of three different Raman-active taggant molecules using three separate inlets (Figure 3a). The taggant molecule solutions are separately filled into the microfluidic channels forming a single character of the desired barcode (Figure 3b). The solutions introduced from the inlet were split into three parallel channels forming the three-line sections of the barcode. The microfluidic mold was designed to enable uniform filling of the channels by equating the hydrodynamic resistance of parallel channels. The calculation of the hydrodynamic pressure was done via Hagen-Poiseuille equation for rectangular channels using the first term of the Taylor series. The resultant channel dimensions are given in Figure 3b for character A. The detailed calculations are given as supplementary information. The mold is removed from the substrate following the complete filling of the channels and evaporation of the solvent (Figure 3c). To prevent any leakage of the taggant solutions from the channels and ensure complete filling of the channels, we used a co-solvent system that consist of 95% water and 5% ethanol. Using purely

water-based solvent hindered complete filling, whereas sole ethanol was prone to leakage. To further enhance the contact between the substrate and mold, the PDMS molds were prepared using a base polymer to curing agent ratio of 15:1 and PMMA slabs were employed to sandwich the substrate and PDMS molds. The thickness of end-grafted polymer is ~8 nm and the largest size of gold nanoparticles is 60 nm. This nanoscopic height difference is easily sealed by the PDMS mold.

A unique advantage of the presented platform is that the barcodes are nearly invisible in the optical microscope (Figure 3d). Mapping the substrate via a Raman microscope reveals the barcodes. The Raman spectra for R6G, MB, and MO are given in Figure 3e. To construct a Raman mapping image, we choose three bands, centered at positions of 1507 cm^{-1}, 1624 cm^{-1}, 1139 cm^{-1} for R6G, MB, MO, respectively. These bands refer to the aromatic C-C stretch peak [32] at 1507 cm^{-1}, the C–C stretching [33] at 1624 cm^{-1}, and azo group bands (ν(Ph-N_2)) [34] at 1139 cm^{-1}, respectively. These bands were chosen to minimize the crosstalk between different taggant molecules. Figure 3f presents the resulting Raman mapping image for a barcode representing ABC letters in Code 93 system. Each character becomes visible after mapping the Raman intensity of the fingerprint vibration of the corresponding taggant molecules.

The enabling idea here is that only the intersection regions of plasmonic arrays with taggant molecules result in intense and spatially defined Raman scattering. In the absence of a taggant molecule, there is no Raman scattering associated with the fingerprint vibrations of the molecule. The weak Raman scattering from taggant molecules in the absence of plasmonic NPs ensures selective Raman scattering intensity in the barcode geometry. The ratio of the Raman scattering intensity from the taggant molecule to the background intensity is roughly 30 times, enabling strong contrast in the Raman mapping images (see supporting Figure S1 for the spectra). An important consideration in visualization and verification of the barcodes in Raman mapping

images is the uniformity of the SERS activity. Raman spectra taken from 20 different positions over the plasmonic arrays for the three taggant molecules showed that the characteristic bands can be clearly distinguished (Figure S2). The standard deviation in the intensity was ~20% of the average intensity.

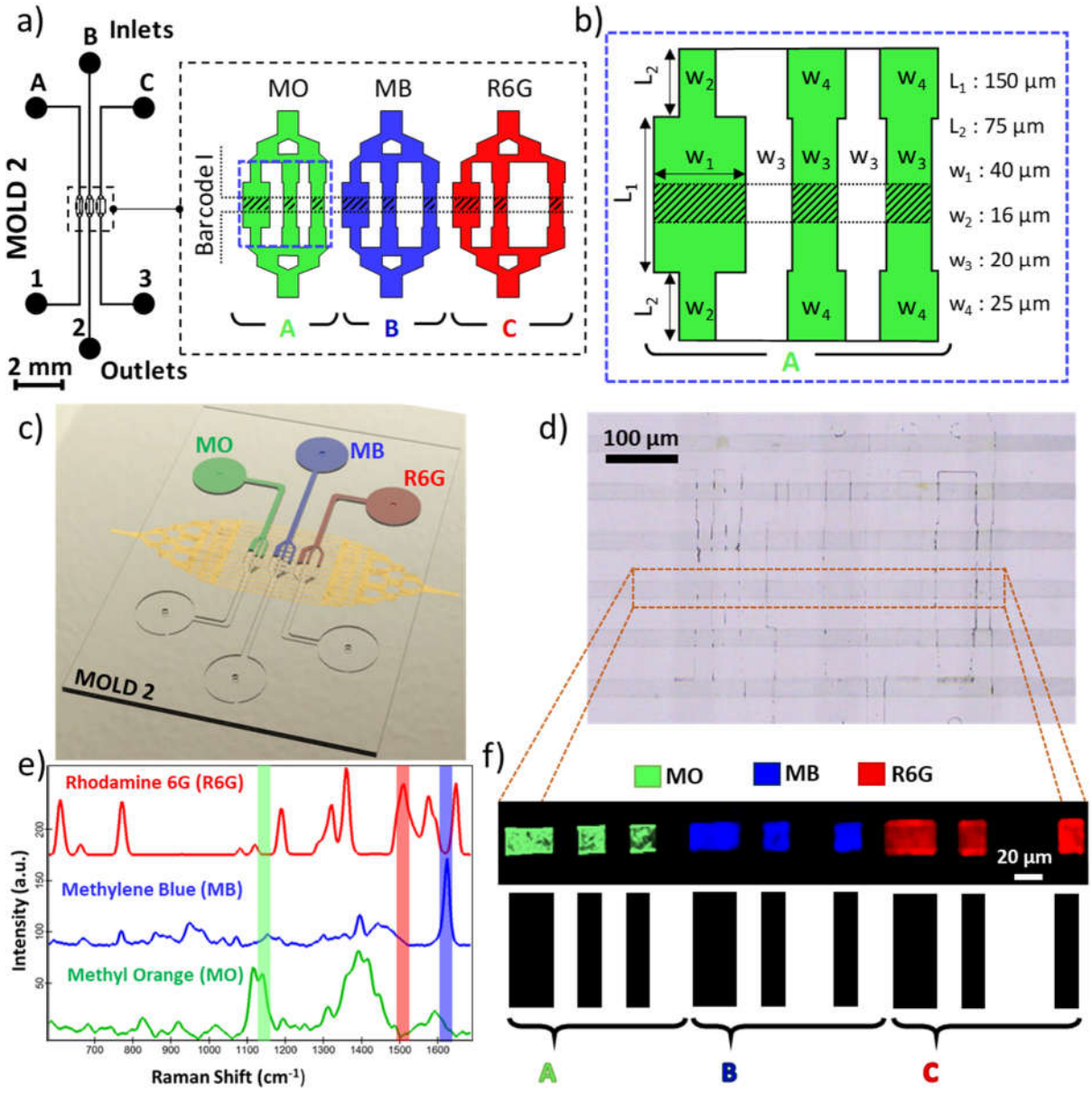

Figure 3. Barcode I. a) Microchannel design, the close-up image shows the manifold-like region corresponding to the section forming the barcode with the underlying plasmonic layer b) The channel dimensions used to form character A in Code 93. c) Schematic illustration for patterning of multiple taggant molecules using Mold 2 on the plasmonic arrays. d) Optical microscope image of substrate following deposition of the taggant molecules. The shaded bands denote the positions of Raman shift used to generate the mapping image. f) The Raman mapping image generated by the spatial variation of the Raman intensity at positions of 1139 cm^{-1} (MO), 1624 cm^{-1} (MB), and 1507 cm^{-1} (R6G). The barcode represents the letters ABC in Code 93.

One approach to further increase the complexity of the barcodes is to use more than one molecule per individual character in the coding system. As demonstrated by Li et al., [22] the coding capacity can be dramatically increased by using different Raman-active taggant molecules for defining bars that represent an individual character. To demonstrate this concept, we designed Mold 3 (Figure 4a, 4b, and 4c) that supplies taggant molecules into closely spaced linear regions using multiple inlets for each solution. Barcodes representing ABC letters were generated using two different taggant molecules, MB and R6G (Figure 4a), patterned by complete filling of the channels followed by evaporation of the solvent. The barcodes were invisible in the optical microscopy image (Figure 4d), where the underlying plasmonic array is discernible. Mapping the Raman scattering intensity of the characteristic peaks of the taggants resulted in verification of the barcodes (Figure 4e). The yellowish appearance of the linear array of gold nanoparticles (Figure 4d) verifies that the particles remain attached to the substrate during the second molding process. The gentle removal of the mold from the substrate and the robust nature of the end-grafted polymers [35] are critical in achieving a stable SERS-active barcode. Note that the adhesion

between the elastomeric PDMS mold and substrate is dependent on the separation velocity of the mold and substrate [36]. At high separation velocities, the adhesion is strong and PDMS can pick-up objects from the substrate, whereas the adhesion is weak when the mold is separated slowly from the substrate.

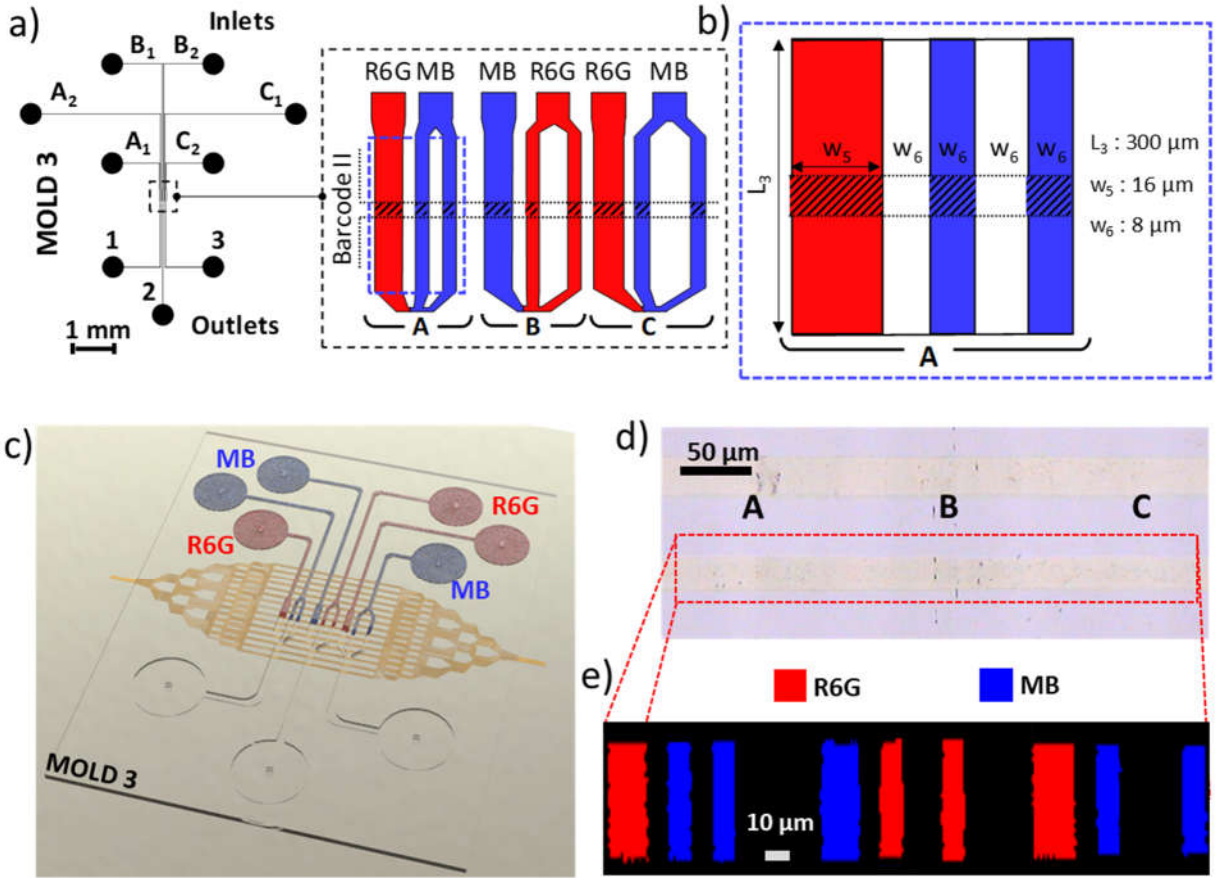

Figure 4. Barcode II. a) Microchannel design, the close-up image shows the region corresponding to the section forming the barcode with the underlying plasmonic layer. b) The channel dimensions used to form character A in Code 93. c) Schematic illustration of patterning multiple Raman-active molecules using Mold 3 on the plasmonic arrays. d) Optical microscope image of the substrate. e) The Raman mapping image generated by using the spatial variation of the Raman intensity at positions of 1624 cm^{-1} (MB) and 1507 cm^{-1} (R6G).

The microfluidic-assisted patterning of the barcode design allows robust and low-cost fabrication and enables generation of barcodes with multi-taggant molecules. An important advantage of the presented approach over other soft lithographic approaches such as microcontact printing [37] is the ability to pattern multiple taggant molecules on the same substrate, a capability that is critical for surface encoding applications. The PDMS molds can be repeatedly used to deposit different molecules, since the molds can survive washing in a series of organic solvents [38]. It is also important to note that the microfluidic approach presented in this study can be extended for a programmable Code 93 barcode generator when it is combined with a valve-equipped design. The laminar flow regime obtained at low Reynolds numbers in microfluidic devices enables co-flow of different fluids as esthetically demonstrated by Folch group [39]. Then, the 9-digit binary form of each character of the barcode can be designed by controlling the plumbing to the channel overlapping with the plasmonic region using microvalves. To define the spaces between the lines, a taggant-free solution can be used. The use of elastomeric valves is a common approach for such advanced plumbing applications, which can also be used to operate the system without an external pump, since peristaltic pumping is easily implemented for such systems [40]. Another advanced feature that can be included in the microfluidic-assisted SERS-active barcode generation is formation of color-gradient barcodes by controlling the concentration of taggant molecules using microfluidic concentration gradient generator designs [41]. The conventional, tree-shape design can be used without sacrificing the robustness and budget-friendliness of the presented approach.

4. Conclusions

This study has shown the use of microfluidic-assisted patterning for fabrication of deterministically encoded surfaces. The spatially and chemically defined linear barcodes offer

unlimited number of opportunities in development of security labels. A unique advantage of the presented approach is that molecular vibration and geometry-based information can be encoded in a small area, which greatly challenge cloning of these security labels. The size of SERS-active linear barcodes is at least an order of magnitude smaller than previous demonstrations [22]. The solution processing based fabrication of linear barcodes from multiple materials can be easily adapted to encoding systems with different authentication mechanisms. A key improvement achieved in this study, in comparison with previous studies [27,31], is the ability to pattern discontinuous patterns through employment of multiple molds on the same substrate. This capability together with the scalability and versatility of the presented approach can find potential uses in different applications that range from electrochemical sensors to electronic devices.

Corresponding authors

* E-mail: onses@erciyes.edu.tr (M.S.O.)

* E-mail: elbuken@unam.bilkent.edu.tr (C.E.)

Notes

Acknowledgments

This work was supported by TUBITAK under Grant No. 115M220. MSO and CE acknowledge the support from The Science Academy, Turkey through the Young Scientist Award Program.

References

[1] R. Dinesh, R.G. Kiran, M. Veena, Classification and Decoding of Barcodes: An Image Processing Approach, in: Lect. Notes Electr. Eng., 2013: pp. 293–307. https://doi.org/10.1007/978-81-322-1143-3_24.

[2] M. Wang, B. Duong, H. Fenniri, M. Su, Nanomaterial-based barcodes, Nanoscale. 7 (2015) 11240–11247. https://doi.org/10.1039/c5nr01948f.

[3] S. Shikha, T. Salafi, J. Cheng, Y. Zhang, Versatile design and synthesis of nano-barcodes, Chem. Soc. Rev. 46 (2017) 7054–7093. https://doi.org/10.1039/C7CS00271H.

[4] P. Kumar, S. Singh, B.K. Gupta, Future prospects of luminescent nanomaterial based security inks: from synthesis to anti-counterfeiting applications, Nanoscale. 8 (2016) 14297–14340. https://doi.org/10.1039/C5NR06965C.

[5] B. Bao, M. Li, Y. Li, J. Jiang, Z. Gu, X. Zhang, L. Jiang, Y. Song, Patterning Fluorescent Quantum Dot Nanocomposites by Reactive Inkjet Printing, Small. 11 (2015) 1649–1654. https://doi.org/10.1002/smll.201403005.

[6] L. Xu, J. Chen, J. Song, J. Li, J. Xue, Y. Dong, B. Cai, Q. Shan, B. Han, H. Zeng, Double-Protected All-Inorganic Perovskite Nanocrystals by Crystalline Matrix and Silica for Triple-Modal Anti-Counterfeiting Codes, ACS Appl. Mater. Interfaces. 9 (2017) 26556–26564. https://doi.org/10.1021/acsami.7b06436.

[7] H. Tan, G. Gong, S. Xie, Y. Song, C. Zhang, N. Li, D. Zhang, L. Xu, J. Xu, J. Zheng, Upconversion Nanoparticles@Carbon Dots@Meso-SiO 2 Sandwiched Core–Shell Nanohybrids with Tunable Dual-Mode Luminescence for 3D Anti-Counterfeiting Barcodes, Langmuir. 35 (2019) 11503–11511.

https://doi.org/10.1021/acs.langmuir.9b01919.

[8] Z. Sun, J. Yang, L. Huai, W. Wang, Z. Ma, J. Sang, J. Zhang, H. Li, Z. Ci, Y. Wang, Spy Must Be Spotted: A Multistimuli-Responsive Luminescent Material for Dynamic Multimodal Anticounterfeiting and Encryption, ACS Appl. Mater. Interfaces. 10 (2018) 21451–21457. https://doi.org/10.1021/acsami.8b08977.

[9] S. Kalytchuk, Y. Wang, K. Poláková, R. Zbořil, Carbon Dot Fluorescence-Lifetime-Encoded Anti-Counterfeiting, ACS Appl. Mater. Interfaces. 10 (2018) 29902–29908. https://doi.org/10.1021/acsami.8b11663.

[10] Q.-Y. Lin, E. Palacios, W. Zhou, Z. Li, J.A. Mason, Z. Liu, H. Lin, P.-C. Chen, V.P. Dravid, K. Aydin, C.A. Mirkin, DNA-Mediated Size-Selective Nanoparticle Assembly for Multiplexed Surface Encoding, Nano Lett. 18 (2018) 2645–2649. https://doi.org/10.1021/acs.nanolett.8b00509.

[11] A.F. Smith, P. Patton, S.E. Skrabalak, Plasmonic Nanoparticles as a Physically Unclonable Function for Responsive Anti-Counterfeit Nanofingerprints, Adv. Funct. Mater. 26 (2016) 1315–1321. https://doi.org/10.1002/adfm.201503989.

[12] Z. Zhang, P. Yang, H. Xu, H. Zheng, Surface enhanced fluorescence and Raman scattering by gold nanoparticle dimers and trimers, J. Appl. Phys. 113 (2013) 033102. https://doi.org/10.1063/1.4776227.

[13] S. Karabel Ocal, J. Patarroyo, N.B. Kiremitler, S. Pekdemir, V.F. Puntes, M.S. Onses, Plasmonic assemblies of gold nanorods on nanoscale patterns of poly(ethylene glycol): Application in surface-enhanced Raman spectroscopy, J. Colloid Interface Sci. 532 (2018)

449–455. https://doi.org/10.1016/j.jcis.2018.07.124.

[14] F.W. King, R.P. Van Duyne, G.C. Schatz, Theory of Raman scattering by molecules adsorbed on electrode surfaces, J. Chem. Phys. 69 (1978) 4472–4481. https://doi.org/10.1063/1.436436.

[15] J. Langer, D. Jimenez de Aberasturi, J. Aizpurua, R.A. Alvarez-Puebla, B. Auguié, J.J. Baumberg, G.C. Bazan, S.E.J. Bell, A. Boisen, A.G. Brolo, J. Choo, D. Cialla-May, V. Deckert, L. Fabris, K. Faulds, F.J. García de Abajo, R. Goodacre, D. Graham, A.J. Haes, C.L. Haynes, C. Huck, T. Itoh, M. Käll, J. Kneipp, N.A. Kotov, H. Kuang, E.C. Le Ru, H.K. Lee, J.-F. Li, X.Y. Ling, S.A. Maier, T. Mayerhöfer, M. Moskovits, K. Murakoshi, J.-M. Nam, S. Nie, Y. Ozaki, I. Pastoriza-Santos, J. Perez-Juste, J. Popp, A. Pucci, S. Reich, B. Ren, G.C. Schatz, T. Shegai, S. Schlücker, L.-L. Tay, K.G. Thomas, Z. Tian, R.P. Van Duyne, T. Vo-Dinh, Y. Wang, K.A. Willets, C. Xu, H. Xu, Y. Xu, Y.S. Yamamoto, B. Zhao, L.M. Liz-Marzán, Present and Future of Surface-Enhanced Raman Scattering, ACS Nano. 14 (2020) 28–117. https://doi.org/10.1021/acsnano.9b04224.

[16] S. Pekdemir, I. Torun, M. Sakir, M. Ruzi, J.A. Rogers, M.S. Onses, Chemical Funneling of Colloidal Gold Nanoparticles on Printed Arrays of End-Grafted Polymers for Plasmonic Applications, ACS Nano. 14 (2020) 8276–8286. https://doi.org/10.1021/acsnano.0c01987.

[17] Y. Zheng, C. Jiang, S.H. Ng, Y. Lu, F. Han, U. Bach, J.J. Gooding, Unclonable Plasmonic Security Labels Achieved by Shadow-Mask-Lithography-Assisted Self-Assembly, Adv. Mater. 28 (2016) 2330–2336. https://doi.org/10.1002/adma.201505022.

[18] Y. Liu, Y.H. Lee, Q. Zhang, Y. Cui, X.Y. Ling, Plasmonic nanopillar arrays encoded with

multiplex molecular information for anti-counterfeiting applications, J. Mater. Chem. C. 4 (2016) 4312–4319. https://doi.org/10.1039/C6TC00682E.

[19] C.L. Lay, C.S.L. Koh, J. Wang, Y.H. Lee, R. Jiang, Y. Yang, Z. Yang, I.Y. Phang, X.Y. Ling, Aluminum nanostructures with strong visible-range SERS activity for versatile micropatterning of molecular security labels, Nanoscale. 10 (2018) 575–581. https://doi.org/10.1039/C7NR07793A.

[20] Y. Cui, I.Y. Phang, Y.H. Lee, M.R. Lee, Q. Zhang, X.Y. Ling, Multiplex plasmonic anti-counterfeiting security labels based on surface-enhanced Raman scattering, Chem. Commun. 51 (2015) 5363–5366. https://doi.org/10.1039/c4cc08596e.

[21] Y. Liu, Y.H. Lee, M.R. Lee, Y. Yang, X.Y. Ling, Flexible Three-Dimensional Anticounterfeiting Plasmonic Security Labels: Utilizing Z -Axis-Dependent SERS Readouts to Encode Multilayered Molecular Information, ACS Photonics. 4 (2017) 2529–2536. https://doi.org/10.1021/acsphotonics.7b00796.

[22] D. Li, L. Tang, J. Wang, X. Liu, Y. Ying, Multidimensional SERS Barcodes on Flexible Patterned Plasmonic Metafilm for Anticounterfeiting Applications, Adv. Opt. Mater. 4 (2016) 1475–1480. https://doi.org/10.1002/adom.201600247.

[23] E. Kim, Y. Xia, G.M. Whitesides, Micromolding in Capillaries: Applications in Materials Science, J. Am. Chem. Soc. 118 (1996) 5722–5731. https://doi.org/10.1021/ja960151v.

[24] M.T. Demko, T.P. Brackbill, A.P. Pisano, Simultaneous Patterning of Nanoparticles and Polymers Using an Evaporation Driven Flow in a Vapor Permeable Template, Langmuir. 28 (2012) 9857–9863. https://doi.org/10.1021/la301587f.

[25] M. Kim, S. Schmitt, J. Choi, J. Krutty, P. Gopalan, From Self-Assembled Monolayers to Coatings: Advances in the Synthesis and Nanobio Applications of Polymer Brushes, Polymers (Basel). 7 (2015) 1346–1378. https://doi.org/10.3390/polym7071346.

[26] S. Pekdemir, S. Karabel, N.B. Kiremitler, X. Liu, P.F. Nealey, M.S. Onses, Modulating the Kinetics of Nanoparticle Adsorption for Simple and High-Yield Fabrication of Plasmonic Heterostructures as SERS Substrates, ChemPhysChem. 18 (2017) 2114–2122. https://doi.org/10.1002/cphc.201700368.

[27] S. Karabel Ocal, S. Pekdemir, M. Serhatlioglu, H.H. Ipekci, E. Sahmetlioglu, I. Narin, F. Duman, C. Elbuken, G. Demirel, M.S. Onses, Eco-Friendly Fabrication of Plasmonically Active Substrates Based on End-Grafted Poly(ethylene glycol) Layers, ACS Sustain. Chem. Eng. 7 (2019) 4315–4324. https://doi.org/10.1021/acssuschemeng.8b06133.

[28] M. Karthikeyan, A. Bender, Encoding and Decoding Graphical Chemical Structures as Two-Dimensional (PDF417) Barcodes, J. Chem. Inf. Model. 45 (2005) 572–580. https://doi.org/10.1021/ci049758i.

[29] R.C. Palmer, The Bar Code Book: Comprehensive Guide to Reading, Printing, Specifying, and Applying Bar Code and Other Machine-Readable Symbols, 4th edition, Helmers Publishing, 2001.

[30] B. Vonhören, M. Langer, D. Abt, C. Barner-Kowollik, B.J. Ravoo, Fast and Simple Preparation of Patterned Surfaces with Hydrophilic Polymer Brushes by Micromolding in Capillaries, Langmuir. 31 (2015) 13625–13631. https://doi.org/10.1021/acs.langmuir.5b03924.

[31] Y. Hung, A. Lu, Y. Chang, J. Huang, J. Chang, L. Li, C. Su, Scalable Patterning of MoS 2 Nanoribbons by Micromolding in Capillaries, ACS Appl. Mater. Interfaces. 8 (2016) 20993–21001. https://doi.org/10.1021/acsami.6b05827.

[32] X.N. He, Y. Gao, M. Mahjouri-Samani, P.N. Black, J. Allen, M. Mitchell, W. Xiong, Y.S. Zhou, L. Jiang, Y.F. Lu, Surface-enhanced Raman spectroscopy using gold-coated horizontally aligned carbon nanotubes, Nanotechnology. 23 (2012) 205702. https://doi.org/10.1088/0957-4484/23/20/205702.

[33] M. Sakir, S. Pekdemir, A. Karatay, B. Küçüköz, H.H. Ipekci, A. Elmali, G. Demirel, M.S. Onses, Fabrication of Plasmonically Active Substrates Using Engineered Silver Nanostructures for SERS Applications, ACS Appl. Mater. Interfaces. 9 (2017) 39795–39803. https://doi.org/10.1021/acsami.7b12279.

[34] O. Siiman, A. Lepp, M. Kerker, Combined surface-enhanced and resonance-Raman scattering from the aspartic acid derivative of methyl orange on colloidal silver, J. Phys. Chem. 87 (1983) 5319–5325. https://doi.org/10.1021/j150644a004.

[35] H. Yilmaz, S. Pekdemir, H.H. Ipekci, N.B. Kiremitler, M. Hancer, M.S. Onses, Ambient, rapid and facile deposition of polymer brushes for immobilization of plasmonic nanoparticles, Appl. Surf. Sci. 385 (2016) 299–307. https://doi.org/10.1016/J.APSUSC.2016.05.132.

[36] X. Feng, M.A. Meitl, A.M. Bowen, Y. Huang, R.G. Nuzzo, J.A. Rogers, Competing Fracture in Kinetically Controlled Transfer Printing, Langmuir. 23 (2007) 12555–12560. https://doi.org/10.1021/la701555n.

[37] A. Perl, D.N. Reinhoudt, J. Huskens, Microcontact Printing: Limitations and Achievements, Adv. Mater. 21 (2009) 2257–2268. https://doi.org/10.1002/adma.200801864.

[38] D.J. Graham, D.D. Price, B.D. Ratner, Solution Assembled and Microcontact Printed Monolayers of Dodecanethiol on Gold: A Multivariate Exploration of Chemistry and Contamination, Langmuir. 18 (2002) 1518–1527. https://doi.org/10.1021/la010059z.

[39] G.A. Cooksey, C.G. Sip, A. Folch, A multi-purpose microfluidic perfusion system with combinatorial choice of inputs, mixtures, gradient patterns, and flow rates, Lab Chip. 9 (2009) 417–426. https://doi.org/10.1039/B806803H.

[40] M.A. Unger, Monolithic Microfabricated Valves and Pumps by Multilayer Soft Lithography, Science 288 (2000) 113–116. https://doi.org/10.1126/science.288.5463.113.

[41] X. Wang, Z. Liu, Y. Pang, Concentration gradient generation methods based on microfluidic systems, RSC Adv. 7 (2017) 29966–29984. https://doi.org/10.1039/C7RA04494A.